



Technical accuracy of the integration of an external ultrasonography system into a navigation platform: effects of ultrasonography probe registration and target detection

Frederic A. Wanis^{1,2} · Lars Wessels^{1,3} · Marcus H. T. Reinges^{1,4} · Eberhard Uhl¹ · Andreas Jödicke^{1,5}

Received: 29 June 2017 / Accepted: 27 November 2017 / Published online: 8 December 2017
© Springer-Verlag GmbH Austria, part of Springer Nature 2017

Abstract

Background Intraoperative navigated ultrasonography has reached clinical acceptance, while published data for the accuracy of some systems are missing. We technically quantified and optimised the accuracy of the integration of an external ultrasonography system into a BrainLab navigation system.

Methods A high-end ultrasonography system (Elegra; Siemens, Erlangen, Germany) was linked to a navigation system (Vector Vision; BrainLab, Munich, Germany). In vitro accuracy and precision was calculated from differences between a real world target (high-precision crosshair phantom) and the ultrasonography image of this target in the navigation coordinate system. The influence of the intrinsic component of the calibration phantom (for ultrasonography probe registration), type of target definition (manual versus automatic) and orientation of the ultrasound probe in relation to the navigation tracking device on accuracy and precision were analysed in different settings (100 measurements for each setting) resembling clinically relevant scenarios in the neurosurgical operating theatre.

Results Line-of-sight angles of 45°, 62° and 90° for the optical tracking of the navigated ultrasonography probe and a distance of 1.8 m revealed best accuracy and precision. Technical accuracy of the integration of ultrasonography into a standard navigation system is high [Euclidean error: median, 0.79 mm; mean, 0.89 ± 0.42 mm for 62° angle; median range: 1.16–1.46 mm; mean range (±SD): 1.22 ± 0.32 mm to 1.46 ± 0.55 mm for grouped analysis of all angles tested]. Software-based automatic target definition improved precision significantly ($p < 0.001$).

Conclusions Integration of an external ultrasonography system into the BrainLab navigation is accurate and precise. By modifying registration (and measurement conditions) via software modification, the in vitro accuracy and precision is improved and requirements for a clinical application are fully met.

Keywords Brain · Navigation · Ultrasonography · Intraoperative · Accuracy

Part of these data were presented by F. A. Wanis at the 65th Annual Meeting of the German Society of Neurosurgery in Dresden, Germany, on 13 May 2014.

✉ Marcus H. T. Reinges
Marcus.Reinges@gesundheitsnord.de

¹ Department of Neurosurgery, Universitätsklinikum Giessen und Marburg GmbH – Standort Giessen, Giessen, Germany

² Department of Neurosurgery, HELIOS Dr. Horst Schmidt Kliniken Wiesbaden, Wiesbaden, Germany

³ Department of Neurosurgery, Charité – Universitätsmedizin Berlin, Berlin, Germany

⁴ Department of Neurosurgery, Gesundheit Nord gGmbH, Klinikum Bremen-Mitte, St.-Jürgen-Str. 1, 28177 Bremen, Germany

⁵ Department of Neurosurgery, Vivantes Klinikum Neukölln, Berlin, Germany

Introduction

Modern neurosurgery very often relies on image guidance (i.e. neuronavigation) based on preoperatively acquired magnetic resonance imaging (MRI) and/or computed tomography (CT) images. Soft-tissue lesions within a soft-tissue organ (brain) located within a water-filled rigid box (skull) are prone to misguidance because of a shift of the lesion (brain shift) related to the bony skull, which serves as the reference for the navigation coordinate system. Brain shift depends on lesion-intrinsic (e.g. cyst, perilesional brain oedema) and intervention-dependent (e.g. head positioning, opening of the dura, release of cerebro-spinal fluid, lesion removal) factors, which can be anticipated in part by the neurosurgeon, but may distract accuracy of the navigation procedure [11, 12, 22, 23, 27, 32].

Intraoperative imaging of the brain in order to correct for brain shift is performed using intraoperative MRI (ioMRI), CT (ioCT) or ultrasonography (ioUS). IoUS is less costly compared with ioMRI, but ioUS scan planes during brain surgery often do not match the routine orthogonal planes of MRI or CT images and are therefore less intuitive to the neurosurgeon [1, 5, 7, 35]. Because of these factors, ioUS was linked to navigation devices by some research groups and are in use in the clinical setting with commercially available systems.

One philosophy of ioUS-navigation pairing is to link an arbitrary ultrasonography system to a navigation system via a calibration procedure of the ultrasonography probe or scan plane [2, 9, 10, 12, 15, 16, 38]. A high calibration accuracy for the ultrasound scan point within the navigation coordinate system is key for clinical use, because the system is expected to show the neurosurgeon a defined point in the real world (e.g. the lesion) within the ultrasound image (with its intrinsic sources of image distortion), which is defined in the navigation coordinate system serving for a surgical pointer or the focal point of the surgical microscope to spot that point in the real world (brain lesion) with highest accuracy.

This in vitro study defines the accuracy of the integration of a standard high-end ultrasonography system linked to a standard neuronavigation system in real-world coordinates.

Materials and methods

For integration of ultrasonography into the neuronavigation system (Vector Vision®; BrainLab, Munich, Germany), a phased-array multifocal ultrasonography probe (7,5 PL 13/9.0; Siemens, Erlangen, Germany) was rigidly fixed to a dedicated position tracker oriented parallel to the ultrasonography plane (Fig. 1). Ultrasonography images were transferred from the ultrasonography system (Sonoline Elegra; Siemens, Erlangen, Germany) to the navigation software via time-coded frame-grabbing. Position of the ultrasonography probe was monitored by an infrared camera system (Polaris; Northern Digital, Bakersfield, CA, USA) attached to the navigation computer (Fujitsu Siemens; Windows XP Version 2002). For accuracy testing, an ultrasonography target (cross-wire) was defined within the coordinate system of the navigation system manually by one observer.

Navigation software

The navigation software (VectorVision®; BrainLab, Munich, Germany) was modified within its ultrasonography-module for study purposes, so that two software versions were compared:

- Standard software vv Cranial 7.5 (*software A*)

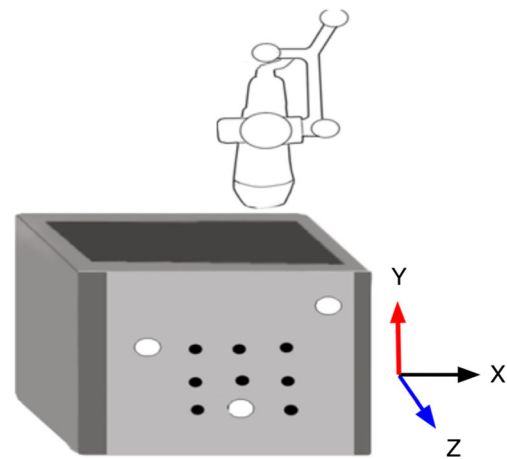


Fig. 1 Navigated ultrasonography: ultrasound probe with navigation tracker. The phantom below (grey, with navigation markers shown as white circles) defines the Cartesian coordinates (X – Z , as depicted). Since the probe tracker is in the direction of the phantom markers, the coordinate system of the ultrasound probe resembles the phantom coordinate system

- Test version vv Cranial 7.81 (*software B*)

The definition of the centre of the cross-wire within the ultrasonography image differed between software versions: with *software A* the target centre had to be defined *manually*, whereas with *software B* the centre was defined *automatically* via a pattern-recognition algorithm of the software.

Registration phantoms

Registration of the ultrasonography probe within the navigation coordinate system was performed via a commercially available phantom, which was modified for study purposes: *standard phantom A* (No. 22530–0; BrainLab, Munich, Germany; Fig. 2a) and *modified phantom B* (No. 22630; BrainLab, Germany). Both phantoms contain nine cross-wire targets. The phantom geometry (height \times width \times depth) is 15.8 cm \times 21.0 cm \times 5.5 cm.

Phantom B differed from *phantom A* by a modification of the urethane filling without intended change of the speed-of-sound characteristics. Gel particles, usually integrated in urethane ultrasonography phantoms in order to resemble ultrasound tissue characteristics more realistically in B-mode images, were removed from the gel. This modification was intended to improve software-based automatic target detection. The material and geometrical orientation of the target wires and their precalibrated crosshairs did not differ between both phantoms.

Probe calibration was performed automatically by software-based target identification within the ultrasonography image of the calibration phantom.

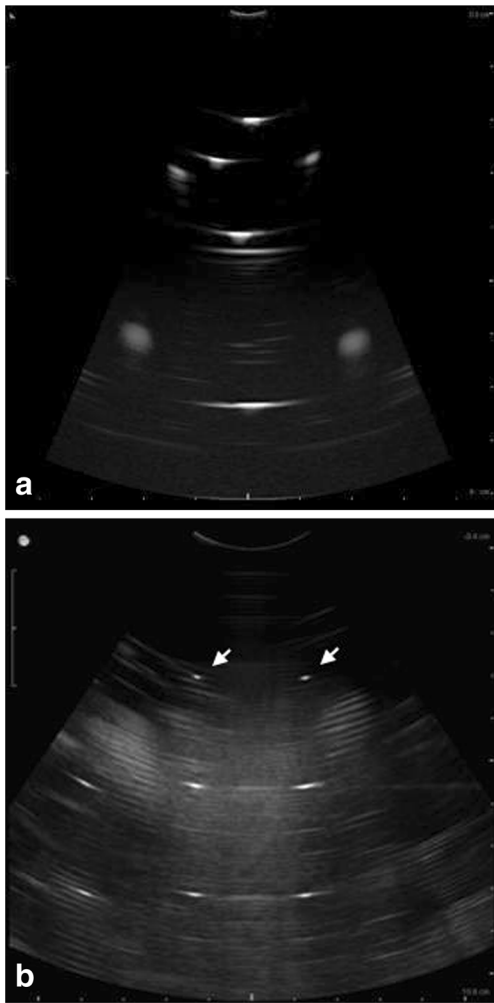


Fig. 2 **a** Ultrasonography image, calibration phantom. Five hyperechoic targets can be seen near to the probe (*top of image*). **b** Ultrasonography image, test phantom. The ultrasonography beam is focused to the top layer of target points (*white arrows*)

Test phantom

Accuracy of the registration and, therefore, of the integration of ultrasonography image data into the navigation coordinate system was tested using a dedicated high-precision test phantom. This rigid phantom contained 18 steel wires defining 27 cross-points as discrete ultrasonography targets. The phantom was equipped with reflective position markers of the navigation system and registered using high-resolution laser-detection. Every single cross-wire position was technically defined within the navigation coordinate system as real world coordinates (BrainLab, Munich, Germany) and served as reference for its identification by ultrasonography (Fig. 2b). The phantom was filled with distilled water (24 °C). Speed of sound was adjusted to 1,480 m/s, accordingly [40].

Differences of the real world coordinates to the coordinates detected by ultrasonography were defined as deviations in millimetres within the Cartesian navigation coordinates (i.e.

X, Y, Z). In addition, the Euclidean error was calculated (Fig. 3), which is very important in the clinical setting.

Navigation coordinates resembled the orientation of the ultrasound plane (and therefore sources of error) as follows: X = lateral direction; Y = axial direction; Z = elevational direction or “slice thickness” (Fig. 4).

Hardware set-up and test sequences

To simulate a neurosurgical set-up during intracranial surgery, the distance and the angle of the patient (target tracker, resembling the test phantom) to the camera of the navigation system (infra-red camera) was modified in five settings:

- 45° angle/1.8 m distance
- 62° angle/1.5 m distance
- 62° angle/1.8 m distance
- 62° angle/2.1 m distance
- 90° angle/1.8 m distance

with the angle defined as horizontal deviation of the line of sight from ground (Fig. 5).

A centre point of the test phantom (P14) was chosen as the ultrasonography target (*set point*; coordinates *see* Table 1; *see* Fig. 3 for illustration). This target was either manually or automatically defined within the ultrasonography image. There were three test sequences:

1. Phantom A/software A (manual target definition)
 - Target definition using five different angles/distances ($n = 100$ for each setting)
2. Phantom A/software B (automatic target definition)
 - Target definition using three different angles / distances ($n = 100$ for each setting)

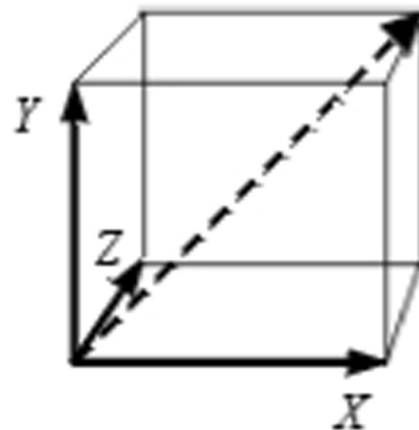


Fig. 3 Euclidean error (graphical illustration of the spatial error as *dashed arrow*)

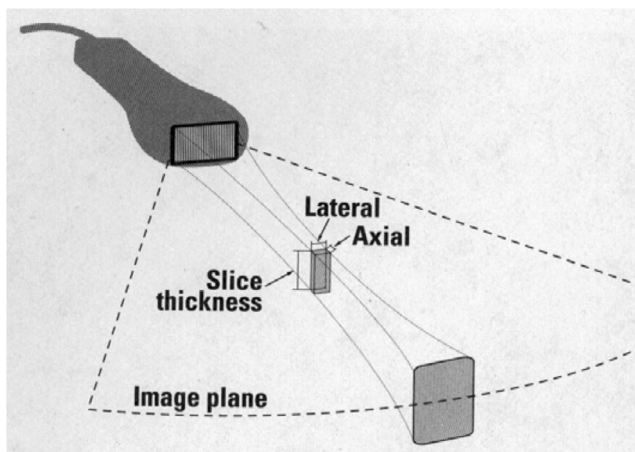
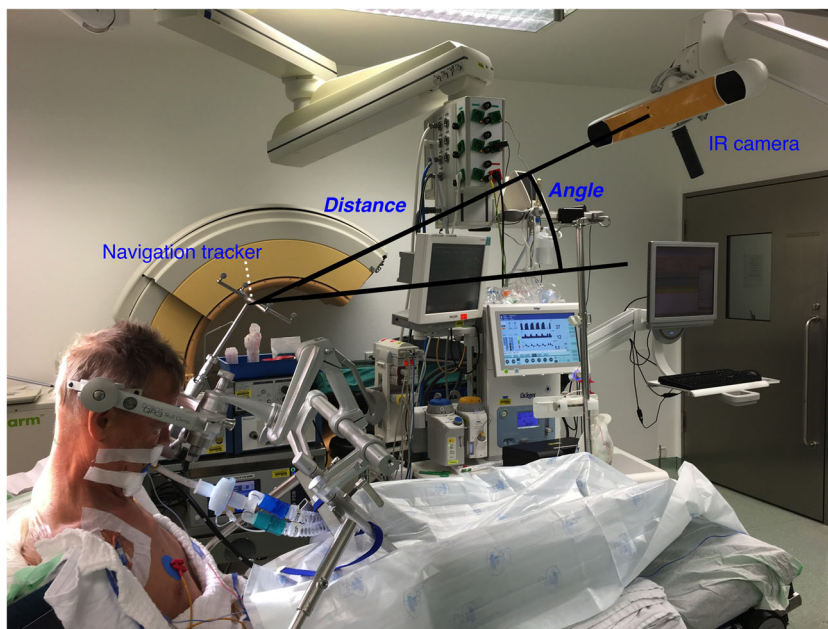


Fig. 4 Ultrasound image plane with according resolutions (lateral, axial, elevational = slice thickness). Reproduced from Zagzebski [40] with permission

3. Phantom B (modified filling)/software B (automatic target definition)
 - Target definition using three different angles/distances ($n = 100$ for each setting)

Sequence 1 and 2 compared the influence of the ultrasonography target definition on target accuracy. Sequence 2 and 3 compared the influence of a modified registration phantom on target accuracy.

Fig. 5 Intraoperative setting of the navigation infra-red camera and the navigation tracker (attached to the patient). Distance and angle are depicted



Statistics

Explorative analysis was performed with the SPSS software (SPSS Statistics 16.0.2 and 21.0; IBM, Albany, NY, USA) and GraphPad Prism (Prism 6.0 g; GraphPad Software, La Jolla, CA, USA). Normal distribution of data was tested using the Kolmogorov-Smirnov test. Intergroup differences were tested using the Wilcoxon test when a normal distribution was rejected. For data with normal distribution, ANOVA was performed (overall intergroup variances), group differences of means were tested using a t -test. For statistical comparison of standard deviations Levene test was used. A p value <0.05 was accepted as a significant group difference.

Results

Sequence 1: characteristics (accuracy, precision) of the basic set-up

Ultrasonography target definition of the set point revealed high accuracy for all settings (Table 1). Manual definition of the target revealed significantly better results at settings $62^\circ/1.5$ m and $62^\circ/1.8$ m compared to all other settings (Euclidean error; $p < 0.001$, Wilcoxon test). Since the Euclidean error between these two settings did not differ significantly, setting $62^\circ/1.8$ m was chosen for further testing because it resembled the clinical intraoperative set-up most due to the larger distance between the operation field and the infra-red camera.

Table 1 Accuracy and precision of ultrasound target detection (mean \pm standard deviation; 45–90°, infra-red camera angle related to the horizontal plane; 1.5–2.1 m, distance between infra-red camera and ultrasound probe/tracker in metres)

	<i>x</i> Mean \pm SD, mm	<i>y</i> Mean \pm SD, mm	<i>z</i> Mean \pm SD, mm	Euclidean error Mean \pm SD, mm
Sequence 1 angle/distance				
45°/1.8	1.21 \pm 1.13	0.5 \pm 0.3	1.06 \pm 0.76	2.02 \pm 0.82
62°/1.5	0.58 \pm 0.73	0.38 \pm 0.23	0.45 \pm 0.66	0.98 \pm 0.85
62°/1.8	0.42 \pm 0.37	0.34 \pm 0.19	0.66 \pm 0.79	1.02 \pm 0.69
62°/2.1	0.59 \pm 0.84	0.52 \pm 0.28	0.68 \pm 0.73	1.27 \pm 0.88
90°/1.8	0.39 \pm 0.24	0.55 \pm 0.16	0.82 \pm 0.69	1.15 \pm 0.60
Sequence 2 angle/distance				
45°/1.8	0.81 \pm 0.26	1.08 \pm 0.05	0.32 \pm 0.24	1.42 \pm 0.18
62°/1.8	0.22 \pm 0.16	0.74 \pm 0.03	0.16 \pm 0.17	0.82 \pm 0.10
90°/1.8	0.24 \pm 0.17	1.25 \pm 0.10	0.54 \pm 0.29	1.42 \pm 0.19
Sequence 3 angle/distance				
45°/1.8	0.62 \pm 0.26	0.24 \pm 0.08	0.59 \pm 0.41	0.96 \pm 0.33
62°/1.8	0.59 \pm 0.37	0.08 \pm 0.06	0.70 \pm 0.47	1.79 \pm 0.43
90°/1.8	1.48 \pm 0.49	0.09 \pm 0.07	0.56 \pm 0.41	1.63 \pm 0.49

Coordinate axes resemble ultrasonography image plane orientation: *x* = lateral direction, *y* = axial direction, *z* = slice thickness. *Sequence 1* phantom A, manual target definition; *Sequence 2* phantom A, automatic target definition; *sequence 3* modified calibration phantom B, automatic target definition

Precision was analysed by comparing standard deviation of the Euclidean error of the different settings. Standard deviation was smallest within the 90°/1.8 m setting, but did not significantly differ from 62°/1.5 m setting. There was no significant difference between 62°/1.5 m and 62°/1.8 m. Therefore, the setting 62°/1.8 m was chosen as reference for further experimental sequences and compared to setting 45°/1.8 m to further test the influence of the line-of-sight angle of the infra-red camera on accuracy and precision.

Sequence 2: influence of ultrasound target definition on accuracy and precision

Ultrasonography target definition of the set point again revealed high accuracy for all three settings (Table 1). Automatic, software-based target definition revealed a significantly higher accuracy ($p < 0.001$; Wilcoxon test) and precision ($p < 0.001$; Levene test) for the Euclidean error of the 62° setting over to the 45° and 90° setting.

Automatic, software-based definition of the target within the ultrasonography image significantly reduced the target data distribution, thereby improving precision, in both settings compared to sequence 1.

Sequence 3: influence of calibration phantom design on accuracy and precision

In this sequence, ultrasonography probe registration was performed using a modified registration phantom (phantom gel

modification). Ultrasonography target definition of the set point using automatic software-based target definition again revealed high accuracy for all three settings tested (Table 1). Euclidean error was significantly lower for the 45°/1.8 m setting compared to 62°/1.8 m and 90°/1.8 m ($p < 0.001$, Wilcoxon test).

Accuracy along the *X*-axis (resembling the lateral ultrasonography direction) and *Z*-axis was significantly reduced the 62° setting only ($p < 0.001$; Wilcoxon test; Table 1), accuracy in along the *Y*-axis (resembling axial ultrasonography direction) was significantly improved in both settings ($p < 0.001$; Wilcoxon test; Table 1). In this sequence, Euclidean error of the 45° setting was significantly more accurate and precise compared to setting 62° and 90° ($p < 0.001$; Wilcoxon test/Levene test).

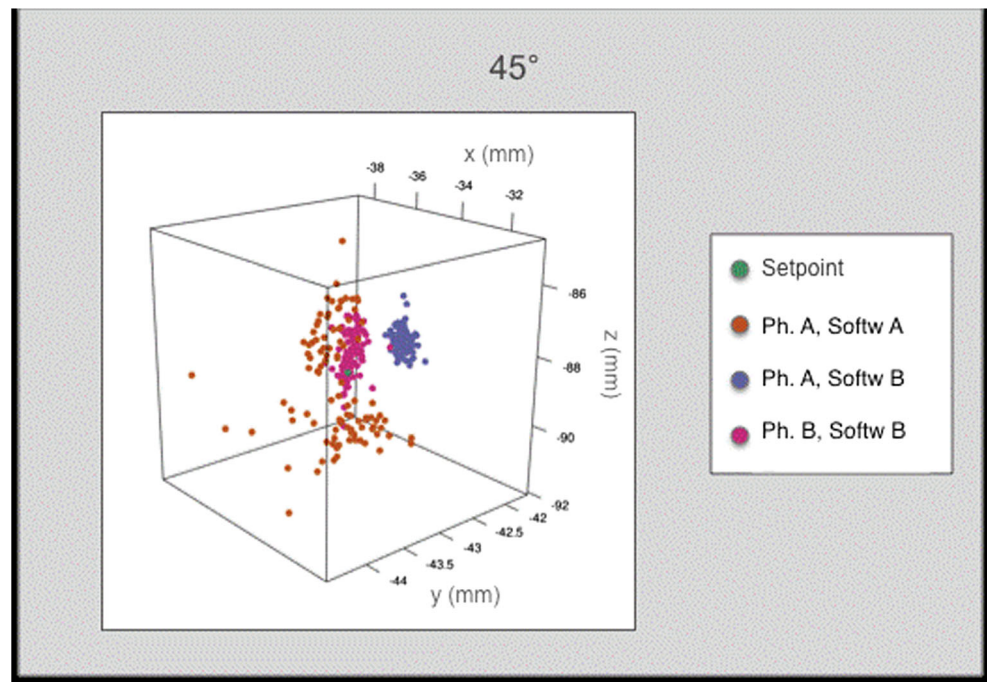
Three-dimensional scatterplots of the sequences 1–3 and the main set-ups of 45° and 62° are given in Figs. 6 and 7, respectively, to visualise the improved precision by the automatic target detection software B.

Intergroup analysis

As Euclidean error counts most in the clinical setting, all data from the settings 45°, 62° and 90° and the three sequences were grouped and analysed to compare either for the influence of angle/distance or calibration phantom/software version on the accuracy of the Euclidean error.

Grouping all sequences, comparative analysis of settings revealed a significantly higher accuracy and precision for the

Fig. 6 Three-dimensional scatterplot, 45° setting (setpoint shown in *green*; sequences 1–3 depicted in *orange*, *blue* and *red*)

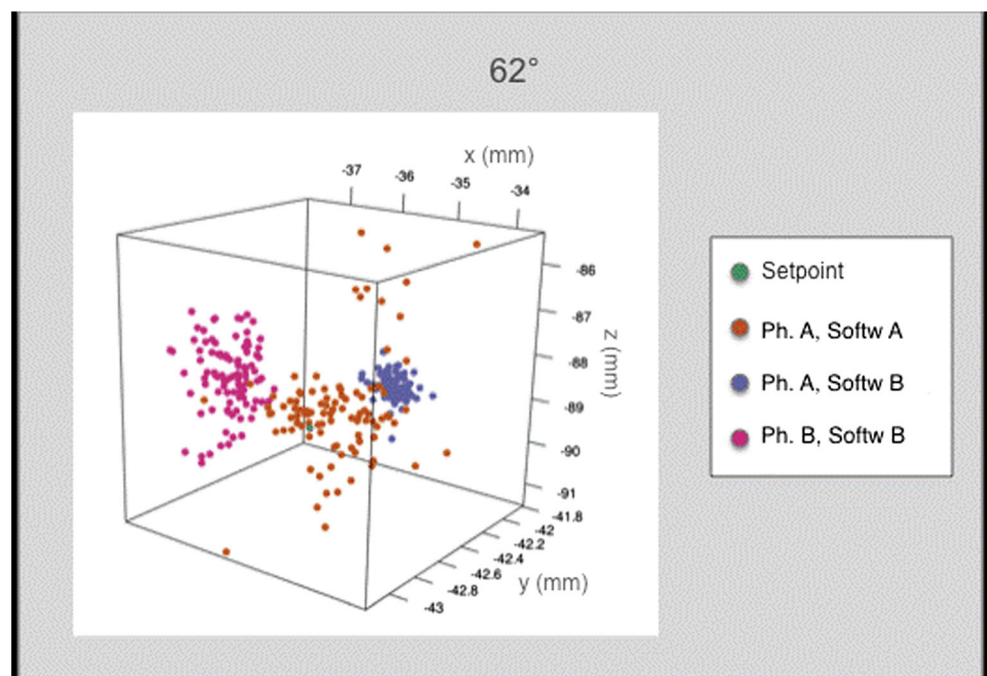


62° setting over the 45° and 90° settings (median, mean \pm SD: 62°, 0.79 mm, 0.89 ± 0.42 mm; 45°, 1.35 mm, 1.46 ± 0.68 ; 90°, 1.37 mm, 1.40 ± 0.50 mm; $p < 0.001$, Wilcoxon test; $p < 0.001$, Levene test, Fig. 8).

Grouping all three settings, analysis of sequences revealed a significantly lower accuracy for the combination of phantom B and an automated, software-based target definition, i.e.

sequence 3. There was no significant difference of medians between sequence 1 and 2 (median, mean \pm SD: sequence 1: 1.16 mm, 1.40 ± 0.84 mm; sequence 2: 1.29 mm, 1.22 ± 0.32 mm; sequence 3: 1.46 mm, 1.46 ± 0.55 mm; $p < 0.001$, Wilcoxon test, Fig. 9). Precision was significantly higher (lower SD) in sequence 2 compared to both other sequences ($p < 0.001$, Levene test).

Fig. 7 Three-dimensional scatterplot, 62° setting (setpoint shown in *green*; sequences 1–3 depicted in *orange*, *blue* and *red*)



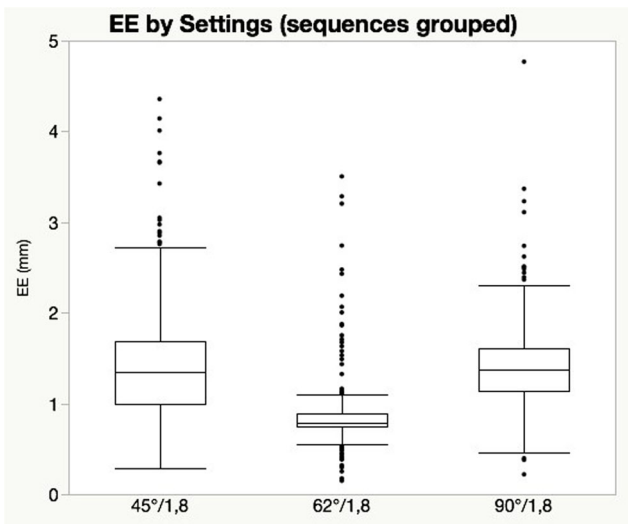


Fig. 8 Grouped analysis of accuracy by angle: Euclidean error (*EE*). The best accuracy and precision is shown for 62° (sequences 1–3 grouped)

Discussion

Accuracy depending on ultrasound data registration in neuronavigation

Very high accuracy and very high reproducibility (i.e. precision) to locate a defined target within the brain is crucial for neuronavigation systems. In case of shifted targets, the target has to be re-identified via an intraoperative imaging modality and defined within its image data set. These image data then serve as the source of navigation guidance and must be

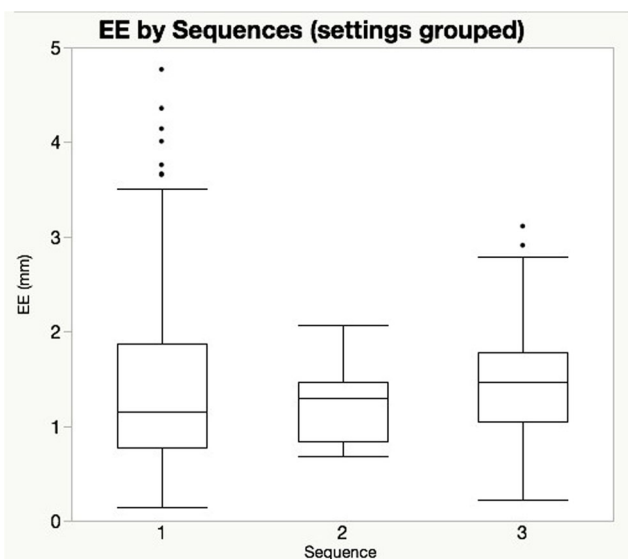


Fig. 9 Grouped analysis of accuracy by sequence: Euclidean error (*EE*). The best accuracy is shown for sequence 1 and 2 (phantom A). The best precision is shown for sequence 2 (phantom A, automatic target definition). All comparable settings (45°/1.8, 62°/1.8, 90°/1.8) are grouped

registered within the navigation coordinate system. This registration is the crucial technical step, which has been tested in this study.

Automatic target detection within the ultrasound image

Target detection within the ultrasound image based on automatic image analysis improved accuracy significantly for all angles and distances tested except for the *X*-axis data within the 62°/1.8 m setting (improvement from 0.42 ± 0.37 mm to 0.22 ± 0.16 mm). Analysis of grouped data from all settings revealed highest accuracy for the combination of phantom A, not dependent from automatic target detection (sequences 1 and 2). Standard deviation, however, was halved and precision significantly improved only with automatic image analysis (sequence 2).

This software algorithm works during the calibration procedure and the accuracy test using the high-precision test phantom. Therefore, accuracy improvement might result from both steps (improved calibration and improved measurement of the calibration result). For the purpose of this study, differentiation of the cause of the improvement is not important. An improved calibration procedure improves accuracy in the clinical setting. Improvement of the target definition during test measurements reduces human error (manual definition of the target point), but does not affect the clinical application. However, it enables a more accurate measurement of the in vitro accuracy of the actual equipment.

Therefore, the implementation of automatic target detection during the calibration procedure retains a high accuracy and improves precision of navigated ultrasonography in this system and is a valid optimisation. Therefore, modification is integrated within the standard BrainLab cranial software.

Gel modification of the calibration phantom

Accuracy improved significantly along the *Y*-axis (i.e. axial direction) by gel-modification in both settings tested (45° and 62°). Accuracy along the *X*- or *Z*-axis was either not improved (45°) or significantly reduced (62°). This result reflects most likely an improved adaption of the speed-of-sound characteristics of the modified phantom gel to the target tissue (i.e. brain), which was not intended initially.

Accuracy of the Euclidean error was improved significantly at 45°, but reduced significantly at 62° compared to the standard calibration phantom A.

Grouped data analysis revealed a significantly higher accuracy for the non-modified Phantom A. This phantom is therefore kept as the standard registration phantom by BrainLab (No. 22530–0).

Optimised angle and distance parameters

Best accuracy and precision was achieved with Euclidean error of median 0.79 mm, 0.89 ± 0.42 mm at 62° . All settings (45° , 62° , 90°) revealed a Euclidean error (medians and means) below 1.5 mm and, therefore, a very high accuracy.

Clinical relevance

Changes in spatial location of intracerebral lesions are influenced by lesion-intrinsic factors such as location of the lesion in relation to the brain surface (deep or superficial) or lesion-induced brain oedema, as well as surgical manipulation [e.g. positioning of the patient's head (elevation, rotation), opening of the dura mater, release of cerebrospinal fluid, removal of the lesion] [1, 11, 23, 27]. A deviation of the real location of the lesion in relation to the location within the navigational location (based on preoperative images) of around 2 mm are accepted early after opening of the dura in superficial intrinsic brain lesions [32]. Therefore, an intraoperative imaging with a target

accuracy below 2 mm for the detection of the lesion would suit the intraoperative surgical needs for microneurosurgery.

This has been achieved by the system tested in this study at clinically relevant settings of infra-red camera distance and angle to the surgical field. In clinical use, camera angles have to be modified according to the positioning of the patient's body, the patient's head and the navigation tracker. It is, therefore, unlikely to precisely match the tested angles of 45° , 62° or 90° , but a range of "optimal" angles seems more important. In our setting, the best angle was identified as 62° .

In a clinically realistic effort–benefit estimation, the accuracy of the system tested was high in its primary design and improved significantly using software based automatic target detection and, less consistently, using an improved calibration phantom.

Integration of ultrasound data into navigation has been studied and published since 1986 [15, 16]. Reconstruction of 3D ultrasound data followed in order to match preoperative CT or MRI data [2, 12]. Clinical application of commercially available systems were implemented in neurosurgical

Table 2 Accuracy of ultrasonography integrated into a neuronavigation system

Authors	Error (mm) mean	Error (mm) SD	Type of phantom	Related target	Data set
Systems without reporting accuracy					
Koivukangas [16]	/	/	/	/	2D/3D
Koivukangas [15]	/	/	/	/	2D
Giorgi [6]	/	/	/	/	2D
Hirschberg [10]	/	/	/	/	2D
Systems with reported accuracy based on image comparison (preoperative image versus intraoperative ultrasound)					
Vince [38]	~4	/	Multiple wire	MRI	2D
Hata [9]	3.1	2.5	Image-matching	MRI	2D
Comeau [4]	~1.3	0.92	Multiple wire	MRI	2D
Schlaier [28]	1.1–1.6	0.6–1.1	Multiple wire	MRI	2D
Keles [14]	~2	/	Not stated	MRI	2D
Sergeeva [29]	1.9	0.97	Not stated	CT	3D
Prada [26]	<3	/	Not stated	MRI	2D
Systems with reported accuracy for defined physical targets					
Trobaugh [34]	1.5	1.5	Cross-wire	Real point	2D
Hartov [8]	2.96	1.85	Cross-wire	Real point	2D
Jödicke [13]	(EE) 2.26	0.97	Cross-wire	Real point	2D
Lindseth [19]	(EE) 1.40	0.45	Cross wire	Real point	3D
Muratore [21]	(EE) 0.39	0.2	Single point	Real point	2D
Trantakis [33]	? 0.8	0.4	Cross-wire	Real point	2D/3D
Wanis et al. (this study)	1.16–1.46 ^a (EE)	0.1	Cross-wire	Real point	2D

EE Euclidean error

^a Range of median

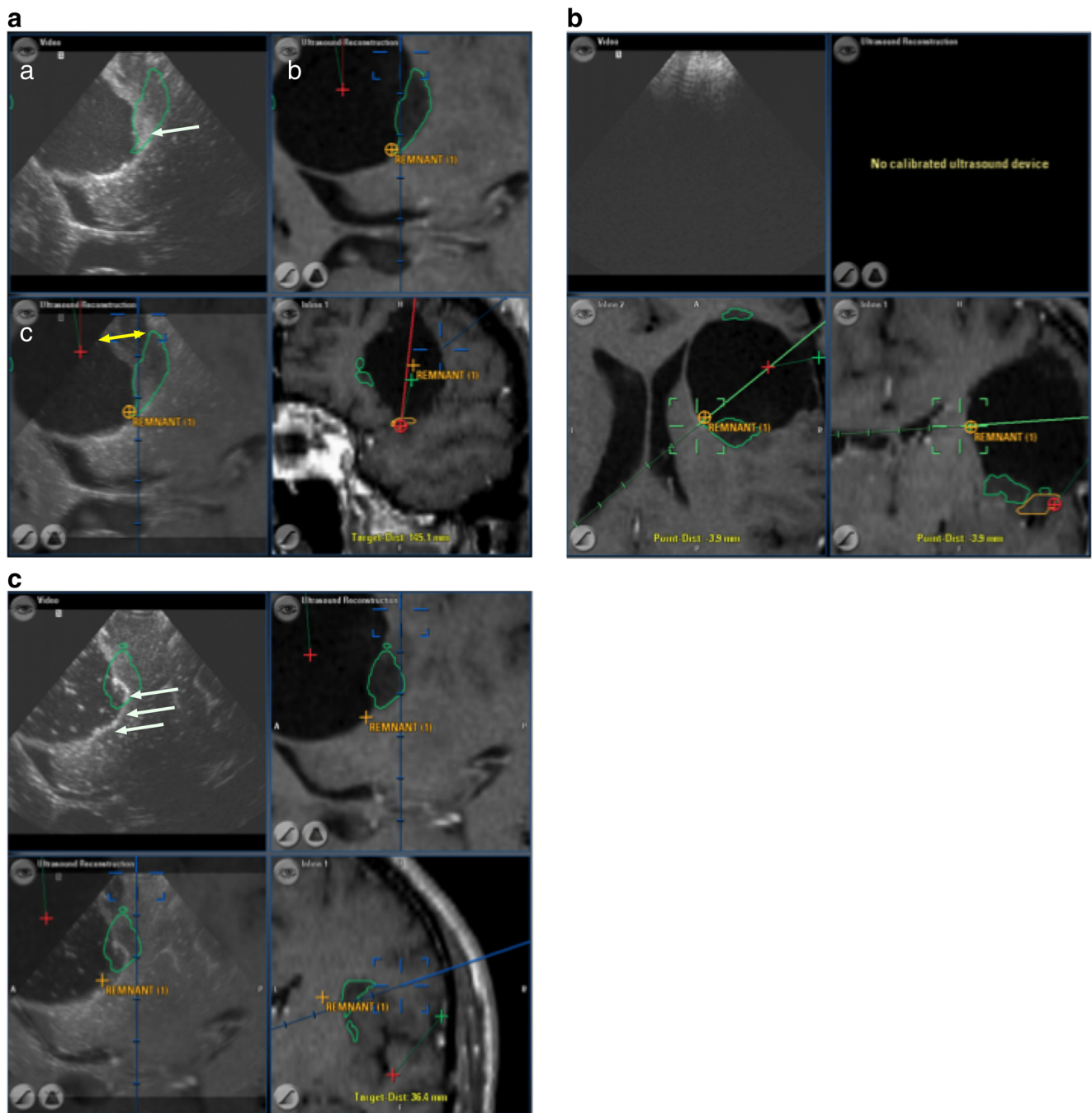


Fig. 10 Ultrasonography-based navigated resection after brain shift. Navigation-screen VV^2 (BrainLab) of the intraoperative situation of near-total resection of a recurrence of a cystic frontal WHO grade II astrocytoma **a** Intraoperative ultrasonography image; **b** corresponding reformatted T1-weighted MR image according to the ultrasound image in **a**. **c** Image overlay of **a** over **b** to visualise image differences. The whole tumour recurrence was marked in *green* (contour) at the preoperative MRI image **b**, which is overlaid on the ultrasonography image **a**. Note the shift of the former resection cavity of approximately 10 mm (*yellow arrow*) by comparing **a** and **b**. The former tumour contour (*green*) now

lies “within” the brain tissue on the ultrasonography image (virtually due to brain shift). After the resection, a small residual tumour remnant (hyperechoic area in the sub-cavity region) is identified using ultrasonography (*white arrow*) and marked with a navigation position marker (remnant 1) in the navigation coordinate system. **b** Identification of the remnant using the navigation pointer (*green crosshair*) and resection of the remnant (no ultrasonography probe used during the resection). **c** Ultrasonography control: complete resection (*white arrows* a clear cavity with typically very sharp hyperechoic rim, no sub-cavity hyperechoic tissue remaining)

departments, including the system tested in this study, and revealed unequivocal results in terms of improvement of intraoperative orientation and resection of intrinsic brain

tumours [20, 25, 30, 31, 35]. This open system (because it allows the integration of an arbitrary ultrasound system by calibration with and data-transfer to the navigation system)

seems to be interesting because it allows for the integration of ultrasound systems already present in the operation room and might therefore be cost saving.

As shown in Table 2, accuracy of different navigated ultrasonography systems was published with differing but improving results over the years. It is important to recognise that the methods of accuracy testing differ [4, 6, 8–10, 13–16, 19, 21, 26, 28, 29, 33, 34, 38]. Highest quality of test results can be expected from in vitro testings comparing a defined point in the ultrasound image with its corresponding point in real world (phantom based testing; last section of Table 2).

Intraoperative comparison of anatomical landmarks is prone to error because clearly defined landmarks with sub-millimetre dimensions are extremely scarce. Prada et al. [26] recently reported a target localisation error below 3 mm for all intraoperative landmarks tested in their abstract, but did not give detailed data in their clinical paper on the method used and the landmarks tested.

The best clinical approximation would be the tributary of a cortical or subcortical artery or vein, which could be compared between two image modalities. This has actually been done on a routine basis by using stand-alone navigation (comparison of brain surface vessel anatomy and MRI vessel anatomy) to verify the reliability of the calibration procedure of the navigation itself [24]. It has not been published so far in detail to study the clinical accuracy of navigated ultrasonography.

Intraoperative accuracy is more than just image overlay of preoperative MRI and ioUS with a similar looking shape of large landmarks. Accuracy must be high enough to spot a small target (i.e. a small tumour remnant at a resection cavity) and to define it within the navigation coordinate system in order to touch it with the navigation pointer (or resection instrument) with less than 2 mm misguidance within the 3D surgical field (Euclidean error; *see* Fig. 10 for a clinical example).

This in vitro study proves that the integration of an external ultrasonography system into a neuronavigation platform for neurosurgical operations can be achieved with very high accuracy. The accuracy measured in our setting is among those reported as highest accuracies in the literature and shows the ongoing improvement of these systems in recent years (*see* Table 2). Given the clinical in vivo accuracy of a navigation system during cranial neurosurgery of 2 mm [32], the additional technical error resulting from ultrasonography integration seems very small. Our data supplemented to the optimisation of the “cranial unlimited” software edition of BrainLab (actually version 3.1).

Other factors, such as the intraoperative delineation of targets (e.g. brain tumours) on the ultrasound image [3, 17, 39] and interpretation of ioUS images by the neurosurgeon [18, 25, 30, 36, 37] seem to be remaining sources of clinical inaccuracy using ultrasonography integrated into navigation and demand further research and training.

Limitations of the present study

In vitro analysis of the accuracy of a navigation system reveals a very high accuracy. In vivo studies suffer from multiple drawbacks, such as a poor definition of suitable target point in the preoperative data set (i.e. brain surface vessel on MR imaging) and on ioUS images, or degradation of the navigation accuracy by intraoperative brain shift. These systematic sources of error can be excluded by in vitro testing, which uncovers the real potential of the combination of integrated ultrasonography in navigation in terms of accuracy. The user has to bear in mind the additional sources of error during the actual surgery.

Conclusions

Integration of an external ultrasonography system into the BrainLab navigation is accurate and precise. By modifying registration (and measurement conditions) via software modification, the in vitro accuracy and precision is improved and requirements for a clinical application are fully met.

Acknowledgments The data presented in this paper are part of the doctoral thesis of F. A. Wanis.

Funding This work was supported by a temporary technical support by BrainLab (Test phantom; infra-red camera; modified registration phantom, test-version of the vvCranial 7.81 software). There are no other affiliations or conflicts of interest.

Compliance with ethical standards

Conflict of interest Frederic A. Wanis has acted as a Consultant to BrainLab since March 2015.

The other authors certify that they have no affiliations with or involvement in any organisation or entity with any financial interest (such as honoraria; educational grants; participation in speakers' bureaus; membership, employment, consultancies, stock ownership, or other equity interest; and expert testimony or patent-licensing arrangements), or non-financial interest (such as personal or professional relationships, affiliations, knowledge or beliefs) in the subject matter or materials discussed in this manuscript.

Ethical approval All procedures performed in studies involving human participants were in accordance with the ethical standards of the institutional and/or national research committee and with the 1964 Helsinki Declaration and its 403 later amendments or comparable ethical standard.

Informed consent Informed consent was obtained from all individual participants included in the study.

References

1. Black PM, Moriarty T, Alexander E, Stieg P, Woodard EJ, Gleason PL, Martin CH, Kikinis R, Schwartz RB, Jolesz FA (1997) Development and implementation of intraoperative magnetic

- resonance imaging and its neurosurgical applications. *Neurosurgery* 41(4):831–842 discussion 842–845
2. Buchholz RD, Yeh DD, Trobaugh J, McDurmont LL, Sturm CD, Baumann C, Henderson JM, Levy A, Kessman P (2005) The correction of stereotactic inaccuracy caused by brain shift using an intraoperative ultrasound device. In: *CVRMed-MRCAS'97*. Springer, Berlin Heidelberg, pp. 459–466
 3. Chacko AG, Kumar NKS, Chacko G, Athyal R, Rajshekhar V (2003) Intraoperative ultrasound in determining the extent of resection of parenchymal brain tumours—a comparative study with computed tomography and histopathology. *Acta Neurochir* 145(9):743–748 discussion 748
 4. Comeau RM, Sadikot AF, Fenster A, Peters TM (2000) Intraoperative ultrasound for guidance and tissue shift correction in image-guided neurosurgery. *Med Phys* 27(4):787–800
 5. Dorward NL, Alberti O, Velani B, Gerritsen FA, Harkness WF, Kitchen ND, Thomas DG (1998) Postimaging brain distortion: magnitude, correlates, and impact on neuronavigation. *J Neurosurg* 88(4):656–662
 6. Giorgi C, Casolino DS (1997) Preliminary clinical experience with intraoperative stereotactic ultrasound imaging. *Stereotact Funct Neurosurg* 68(1–4 Pt 1):54–58
 7. Hammoud MA, Ligon BL, elSouki R, Shi WM, Schomer DF, Sawaya R (1996) Use of intraoperative ultrasound for localizing tumors and determining the extent of resection: a comparative study with magnetic resonance imaging. *J Neurosurg* 84(5):737–741
 8. Hartov A, Eisner SD, David RW, Paulsen KD, Platenik LA, Miga MI (1999) Error analysis for a free-hand three-dimensional ultrasound system for neuronavigation. *Neurosurg Focus* 6(3):E7
 9. Hata N, Dohi T, Iseki H, Takakura K (1997) Development of a frameless and armless stereotactic neuronavigation system with ultrasonographic registration. *Neurosurgery* 41(3):608–613 discussion 613–614
 10. Hirschberg H, Unsgaard G (1997) Incorporation of ultrasonic imaging in an optically coupled frameless stereotactic system. *Acta Neurochir Suppl* 68:75–80
 11. Hu J, Jin X, Lee JB, Zhang L, Chaudhary V, Guthikonda M, Yang KH, King AI (2007) Intraoperative brain shift prediction using a 3D inhomogeneous patient-specific finite element model. *J Neurosurg* 106(1):164–169
 12. Jödicke A, Deinsberger W, Erbe H, Kriete A, Böker D-K (1998) Intraoperative three-dimensional ultrasonography: an approach to register brain shift using multidimensional image processing. *Minim Invasive Neurosurg* 41(1):13–19
 13. Jödicke A, Springer T, Böker D-K (2004) Real-time integration of ultrasound into neuronavigation: technical accuracy using a light-emitting-diode-based navigation system. *Acta Neurochir* 146(11):1211–1220
 14. Keles GE, Lamborn KR, Berger MS (2003) Coregistration accuracy and detection of brain shift using intraoperative sononavigation during resection of hemispheric tumors. *Neurosurgery* 53(3):556–562 discussion 562–564
 15. Koivukangas J, Louhisalmi Y, Alakuijala J, Oikarinen J (1993) Ultrasound-controlled neuronavigator-guided brain surgery. *J Neurosurg* 79(1):36–42
 16. Koivukangas J, Ylitalo J, Alasaarela E, Tauriainen A (1986) Three-dimensional ultrasound imaging of brain for neurosurgery. *Ann Clin Res* 18 Suppl 47:65–72
 17. Le Roux PD, Berger MS, Wang K, Mack LA, Ojemann GA (1992) Low grade gliomas: comparison of intraoperative ultrasound characteristics with preoperative imaging studies. *J Neuro-Oncol* 13(2):189–198
 18. Lindner D, Trantakis C, Renner C, Arnold S, Schmitgen A, Schneider J, Meixensberger J (2006) Application of intraoperative 3D ultrasound during navigated tumor resection. *Minim Invasive Neurosurg* 49(4):197–202
 19. Lindseth F, Langø T, Bang J, Nagelhus Hernes TA (2002) Accuracy evaluation of a 3D ultrasound-based Neuronavigation system. *Comput Aided Surg* 7(4):197–222
 20. Moiyadi AV, Shetty PM, Mahajan A, Udare A, Sridhar E (2013) Usefulness of three-dimensional navigable intraoperative ultrasound in resection of brain tumors with a special emphasis on malignant gliomas. *Acta Neurochir* 155(12):2217–2225
 21. Muratore DM, Galloway RL (2001) Beam calibration without a phantom for creating a 3-D freehand ultrasound system. *Ultrasound Med Biol* 27(11):1557–1566
 22. Nabavi A, Black PM, Gering DT et al (2001) Serial intraoperative magnetic resonance imaging of brain shift. *Neurosurgery* 48(4):787–797 discussion 797–798
 23. Nimsy C, Ganslandt O, Cerny S, Hastreiter P, Greiner G, Fahlbusch R (2000) Quantification of, visualization of, and compensation for brain shift using intraoperative magnetic resonance imaging. *Neurosurgery* 47(5):1070–1079 discussion 1079–1080
 24. Pennec X, Cachier P, Ayache N (2003) Tracking brain deformations in time sequences of 3D US images. *Pattern Recogn Lett* 24(4–5):801–813
 25. Petridis AK, Anokhin M, Vavruska J, Mahvash M, Scholz M (2015) The value of intraoperative sonography in low grade glioma surgery. *Clin Neurol Neurosurg* 131:64–68
 26. Prada F, Del Bene M, Mattei L, Lodigiani L, DeBenedictis S, Kolev V, Vetrano I, Solbiati L, Sakas G, DiMeco F (2015) Preoperative magnetic resonance and intraoperative ultrasound fusion imaging for real-time neuronavigation in brain tumor surgery. *Ultraschall Med* 36(2):174–186
 27. Reinges MHT, Nguyen H-H, Krings T, Hütter B-O, Rohde V, Gilsbach JM (2004) Course of brain shift during microsurgical resection of supratentorial cerebral lesions: limits of conventional neuronavigation. *Acta Neurochir* 146(4):369–377 discussion 377
 28. Schlaier JR, Wamat J, Dorenbeck U, Proescholdt M, Schebesch K-M, Brawanski A (2004) Image fusion of MR images and real-time ultrasonography: evaluation of fusion accuracy combining two commercial instruments, a neuronavigation system and a ultrasound system. *Acta Neurochir* 146(3):271–276 discussion 276–277
 29. Sergeeva O, Uhlemann F, Schackert G, Hergeth C, Morgenstem U, Steinmeier R (2006) Integration of intraoperative 3D-ultrasound in a commercial navigation system. *Zentralbl Neurochir* 67(4):197–203
 30. Serra C, Stauffer A, Actor B, Burkhardt J-K, Ulrich NH-B, Bernays R-L, Bozinov O (2012) Intraoperative high frequency ultrasound in intracerebral high-grade tumors. *Ultraschall Med* 33(7):E306–E312
 31. Singhal A, Ross Hengel A, Steinbok P, Doug Cochrane D (2015) Intraoperative ultrasound in pediatric brain tumors: does the surgeon get it right? *Childs Nerv Syst* 31(12):2353–2357
 32. Stieglitz LH, Fichtner J, Andres R, Schucht P, Krähenbühl A-K, Raabe A, Beck J (2013) The silent loss of neuronavigation accuracy: a systematic retrospective analysis of factors influencing the mismatch of frameless stereotactic systems in cranial neurosurgery. *Neurosurgery* 72(5):796–807
 33. Trantakis C, Meixensberger J, Lindner D, Strauss G, Grunst G, Schmitgen A, Arnold S (2002) Iterative neuronavigation using 3D ultrasound. A feasibility study. *Neurol Res* 24(7):666–670
 34. Trobaugh JW, Trobaugh DJ, Richard WD (1994) Three-dimensional imaging with stereotactic ultrasonography. *Comput Med Imaging Graph* 18(5):315–323
 35. Tronnier VM, Bonsanto MM, Staubert A, Knauth M, Kunze S, Wirtz CR (2001) Comparison of intraoperative MR imaging and 3D-navigated ultrasonography in the detection and resection control of lesions. *Neurosurg Focus* 10(2):E3
 36. Unsgaard G, Rygh OM, Selbekk T, Müller TB, Kolstad F, Lindseth F, Hernes TAN (2006) Intra-operative 3D ultrasound in neurosurgery. *Acta Neurochir* 148(3):235–253 discussion 253
 37. Unsgaard G, Gronningsaeter A, Ommedal S, Nagelhus Hernes TA (2002) Brain operations guided by real-time two-dimensional

- ultrasound: new possibilities as a result of improved image quality. *Neurosurgery* 51(2):402–411 discussion 411–412
38. Vince G, Krone A, Woydt M, Roosen K (1998) Real time ultrasound fusion in optical tracking MR/CT image guided surgery. In: *Proceedings of the XIII Congress of the European Society for Stereotactic and Functional Neurosurgery, Freiburg, 20-23 September 1998*
 39. Woydt M, Krone A, Becker G, Schmidt K, Roggendorf W, Roosen K (1996) Correlation of intra-operative ultrasound with histopathologic findings after tumour resection in supratentorial gliomas. A method to improve gross total tumour resection. *Acta Neurochir* 138(12):1391–1398
 40. Zagzebski JA (1996) *Essentials of ultrasound physics*. Mosby, St. Louis, p 40